Paper
Int'l J. of Aeronautical & Space Sci. 18(4), 614–622 (2017)
DOI: http://dx.doi.org/10.5139/IJASS.2017.18.4.614

IJASS
International Journal of Aeronautical and Space Sciences

A Study on the Aerodynamic Drag of Transonic Vehicle in Evacuated Tube Using Computational Fluid Dynamics

Hyungmin Kang*

Department of Mechanical Engineering, Dongyang Mirae University, Seoul 08221, Republic of Korea

Yingmei Jin and Hyeokbin Kwon*****

Department of Transportation System Engineering, Korea National University of Transportation, Gyeonggi-do 16106, Republic of Korea

Kyuhong Kim*

Mechanical and Aerospace Engineering, Seoul National University, Seoul 08826, Republic of Korea

Abstract

The characteristics of aerodynamic drag for Transonic Vehicle in Evacuated Tube was investigated using computational fluid dynamics. At first, parametric study on the system was performed according to the Mach number of the vehicle's speed ($Mach_v$), evacuated pressure of the tube (Pre_t), and blockage ratio (BR) between the vehicle and tube via axisymmetric flow analysis; the $Mach_v$ ranged from 0.3 to 1.0. The Pre_t was 100, 1,000 and 10,000 Pa and the BR was 0.1, 0.2, and 0.4. In the calculations, the aerodynamic drag of the vehicle was larger when the BR and the pressure became larger. Concerning the $Mach_v$, the drag coefficient (C_d) became the maximum when the $Mach_v$ was near the Kantrowitz limit and decreased, which showed the typical transonic flow pattern. Then, three dimensional flow analysis was performed by changing the $Mach_v$ from 0.3 to 1.0 and setting the BR and the Pre_t as 0.34 and 100 Pa, respectively by referring the Hyperloop Alpha documentation. From the calculations, the C_d from three dimensional flow simulations were somewhat larger than those of axisymmetric ones because of the eccentricity of the vehicle inside the tube. However, the pattern of C_d according to the $Mach_v$ was compatible with that of axisymmetric ones.

Key words: Aerodynamic drag, Computational flow dynamics, Transonic vehicle, Evacuated tube, High-speed trains

Nomenclature

BR	=	Blockage ratio between tube and the vehicle
C_d	=	Drag coefficient
$Mach_{in}$	=	Mach number of inflow speed in front of the vehicle
$Mach_{local}$	=	Local Mach number of the flow
$Mach_v$	=	Mach number of vehicle's speed
Pre_t	=	Evacuated pressure inside the tube

1. Introduction

Using evacuated tube or tunnel as a transportation mode is an old but fascinating idea since Robert H. Goddard, a rocket pioneer proposed in 1909 [1]. Potentially, it can dramatically reduce the aerodynamic drag and prevent aero-acoustic noise from radiating around trackside environments which are the most limiting factors for speed-up of surface vehicles. From 1966 to 1969, research on tube-vehicle system has been conducted by Federal Railroad Administration of United

* Assistant Professor
** Ph. D Student
*** Professor
**** Professor, Corresponding author: hbkwon@ut.ac.kr

Received: October 24, 2017 Revised: November 7, 2017 Accepted: November 7, 2017

http://ijass.org pISSN: 2093-274x eISSN: 2093-2480

States [2] to investigate the feasibility of various concepts both with atmospheric and evacuated tube. Fundamental aerodynamic researches have also been conducted using experimental facilities and the aerodynamic drag of vehicle in tube has been investigated varying model configurations under wide range of Mach number and Reynolds number. Swissmetro [3] is a concept of ultra high speed maglev in evacuated tunnel studied by EPFL in Swiss. It is a network transportation system between cities with a commercial speed of 400 km/h employing two unidirectional tunnels of small diameter around 5 m with partial vacuum of 0.1 atm. Aerodynamic aspects including blockage ratio, partial vacuum, aerodynamic drag have been studied during the main study in between 1994 and 1999. In the early 2000s, the northeast Asian countries have also been interested in this transportation system and several studies have been conducted [4-6]. Although the studies deduced positive feasibilities and hopeful prospects, most of the studies had not progressed further because it needs huge amount of costs for development as well as for implementation.

In 2013, an innovative concept of Hyperloop has been proposed by SpaceX as an alternative to the California high speed rail project between Los Angeles and San Francisco [7]. The main difference of the Hyperloop system from the precedent concepts is that its maximum speed is about 1220km/h which corresponds to Mach number 0.91 while that the others are not more than 700km/h. The very high speed of Hyperloop significantly enhances the utility as a transportation system because it can fully cover the speed between the high-speed trains and jet planes. An inevitable problem for transonic aviation in tube, so called Kantrowitz limit [8] has been solved by applying compressor at the nose of the pod in Hyperloop concept. In addition, downsizing of the system by applying 2.23 m-diameter which is less than the half of Swissmetro can reduce the construction cost and makes Hyperloop more promising.

The role of aerodynamics of vehicles in evacuated tube is very important because the original idea of reducing aerodynamic drag by decreasing air density comes from aerodynamics. Aerodynamics also determines governing system parameters such as tube diameter, vacuum level in tube. For Hyperloop, aerodynamics becomes more important because additional consideration should payed to compressor.

However, the flow regime of Hyperloop is unconventional with very low Reynolds numbers around 2.8×10^4 and with high Mach numbers about 0.91; the pressure of the air inside the tube is 100 Pa and the temperature of the air is 20 ^{o}C. In addition, the flow disturbances by vehicle are enhanced between tube wall and the train and it propagates far away along the tube, which increase difficulties in both experimental and numerical approaches.

In this study, the aerodynamic drag of transonic vehicle in evacuated tube has been studied varying vehicle speed and evacuation level. The effects of Mach number and Reynolds number on the aerodynamic drag of the vehicle has been discussed.

2. Axisymmetric flow simulations of the transonic vehicle-evacuated tube system

2.1 Steady state analysis of the axisymmetric flow in transonic vehicle-evacuated tube system

Generally, when a vehicle travels at a high speed in a stationary state, compressive waves are generated in front of the vehicle, expansion waves are generated in the rear of the vehicle, and propagate to the front and rear respectively. These wave propagations cause the fluctuation of the air in the tube, which is very important in the calculation of the dynamic stability of the vehicle. Especially, the target speed of the transonic vehicle is very high, which may cause strong coupling of wave propagation and shock and results in the strong flow separation and the damage of the dynamic stability of the vehicle. Therefore, unsteady flow simulation should be performed in the transonic vehicle-evacuated tube system and the entire computational domain should be as the distance to which the front and rear pressure waves are propagated. However, unsteady calculation of the vehicle inside of the tube requires a lot of calculation resources.

In this research, our main interest is the parametric study of the design parameters for the systematic design of the transonic vehicle traveling in the tube and the variation of aerodynamic coefficient such as drag coefficient (C_d); steady state calculation can be a good solution for initial design stage. That is, in the evacuated tube system, the pressure of front of the vehicle remains high because of compression wave and that of rear of the vehicle does low because of expansion wave. And the general tube system is very long; the pressure difference of front and rear part of the vehicle is maintained before the reflection of the waves at the exit of the tube and come back to the vehicle. Thus, it is possible to assume that the flow inside the tube is steady state; the aerodynamic characteristics such as the pressure difference between the front and rear part of the vehicle, the aerodynamic drag and C_d can be sufficiently utilized. Therefore in this study, the parametric study on the variation of drag and C_d of the transonic vehicle was done through axisymmetric, steady state calculations according

to the variation of evacuated pressure inside the tube (Pre_t), blockage ratio (BR) between tube and the vehicle, and the Mach number of the vehicle's speed ($Mach_v$).

2.2 Kantrowitz limit

When the vehicle travels inside the tube system, choking occurs in the flow around the vehicle if it exceeds a certain speed by the compressibility of the air. This choking phenomenon is strongly influenced by the BR and Mach number of inflow speed in front of the vehicle ($Mach_{in}$). There is a maximum $Mach_{in}$ of the vehicle in which choking occurs for a given BR [7-9]. At this time, the local Mach number of the flow ($Mach_{local}$) somewhere around the vehicle becomes 1 and the aerodynamic drag increases sharply due to a large pressure rise in the front part of the vehicle. The Kantrowitz limit is defined as the maximum $Mach_{in}$ of the vehicle when $Mach_{local}$ somewhere around the vehicle is 1 and the choking occurs in the given BR [7-10].

The details of the derivation of Kantrowitz limit is as following; assume a fluid enters an internally contracting nozzle at A0, and passes through a throat at A1 as Fig. 1. Due to conservation of mass flow rate within the nozzle and throat, Eq. (1) is satisfied.

$$\dot{m}_0 = \dot{m}_1. \tag{1}$$

For an ideal gas, the mass flow rate can be derived from the isentropic flow relations and equation of state as Eq. (2).

$$\dot{m} = \sqrt{\frac{\gamma}{R}} M \left(1 + \frac{\gamma-1}{2} M^2\right)^{-\frac{\gamma+1}{2(\gamma-1)}} \cdot \left(\frac{p_t A}{\sqrt{T_t}}\right), \tag{2}$$

where p_t is the stagnation pressure, T_t is the stagnation temperature, A is the cross-section area, M is the Mach number, R is the gas constant and γ is the specific heat ratio of air.

If T_t, R, and γ are set as constant, following Eq. (3) can be derived.

$$M_0 \left(1 + \frac{\gamma-1}{2} M_0^2\right)^{-\frac{\gamma+1}{2(\gamma-1)}} p_{t0} A_0 = M_1 \left(1 + \frac{\gamma-1}{2} M_1^2\right)^{-\frac{\gamma+1}{2(\gamma-1)}} p_{t1} A_1. \tag{3}$$

By solving Eq. (3) for $\frac{A_1}{A_0}$, then Eq. (3) can be changed as Eq. (4).

$$\frac{A_1}{A_0} = \frac{M_0}{M_1} \frac{p_{t0}}{p_{t1}} \left(\frac{1+\frac{\gamma-1}{2}M_0^2}{1+\frac{\gamma-1}{2}M_1^2}\right)^{-\frac{\gamma+1}{2(\gamma-1)}}. \tag{4}$$

If the normal shock occurs, the M_1 at the throat is 1 and the pressures between the nozzle and throat are related through normal shock relations as Eq. (5) [8].

$$\frac{p_{t0}}{p_{t1}} = \left(\frac{(\gamma+1)M_0^2}{(\gamma-1)M_0^2+2}\right)^{-\frac{\gamma}{\gamma-1}} \left(\frac{\gamma+1}{2\gamma M_0^2-(\gamma-1)}\right)^{-\frac{1}{\gamma-1}}. \tag{5}$$

From Eq. (4) and (5), the equation of the Kantrowitz limit can be derived as Eq. (6) [10].

$$\frac{A_1}{A_0} = M_0 \left(\frac{\gamma+1}{(\gamma-1)M_0^2+2}\right)^{\frac{\gamma+1}{2(\gamma-1)}} \left(\frac{(\gamma+1)M_0^2}{(\gamma-1)M_0^2+2}\right)^{\frac{-\gamma}{\gamma-1}} \left(\frac{\gamma+1}{2\gamma M_0^2-(\gamma-1)}\right)^{-\frac{1}{\gamma-1}}. \tag{6}$$

In case of vehicle in the tube, $\frac{A_1}{A_0}$ and M_0 are the same as the ratio of tube area to bypass area around the vehicle as $\frac{A_{bypass}}{A_{tube}}$ and $Mach_{in}$, respectively as Fig. 1. Therefore, Eq. (6) can be rewritten as Eq. (7).

$$\frac{A_{bypass}}{A_{tube}} = \left[\frac{\gamma-1}{\gamma+1}\right]^{0.5} \left[\frac{2\gamma}{\gamma+1}\right]^{\frac{1}{\gamma-1}} \left[1 + \frac{2}{\gamma-1}\frac{1}{Mach_{in}^2}\right]^{0.5} \left[1 - \frac{\gamma-1}{2\gamma}\frac{1}{Mach_{in}^2}\right]^{\frac{1}{\gamma-1}}. \tag{7}$$

Then, the BR between the vehicle and tube can be expressed as Eq. (8).

$$BR = \frac{A_{vehicle}}{A_{tube}} = 1 - \frac{A_{bypass}}{A_{tube}}. \tag{8}$$

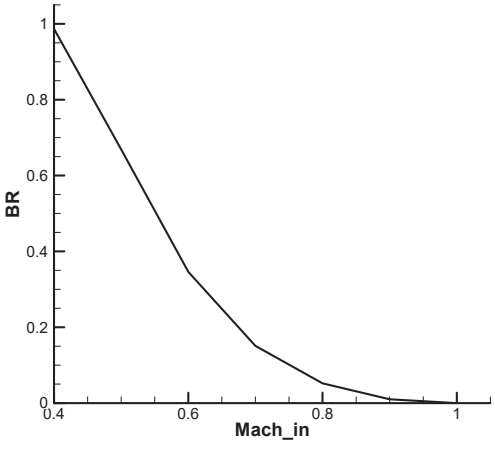

Fig. 2. Illustration of the Kantrowitz limit

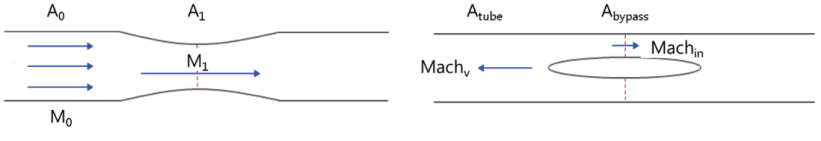

Fig. 1. Schematic diagram of an internally contracting nozzle and evacuated tube system

From the equations, the BR according to the Kantrowitz limit, that is the maximum $Mach_{in}$, is shown in Fig. 2. Here, the BR of the Hyperloop alpha is about 0.36 and $\frac{A_{bypass}}{A_{tube}}$ is 0.64; when applying the equations of Kantrowitz limit to the Hyperloop alpha, the Kantrowitz limit of the Hyperloop alpha is 0.595 and the operating speed of Hyperloop alpha ($Mach_v$ is 0.91) exceeds the limit.

Generally, there are three ways to avoid the Kantrowitz limit in the tube system; the first is to decrease the $Mach_v$ of the vehicle inside the tube, which can decrease the effectiveness of the transonic vehicle-evacuated tube system. The second is to decrease the BR between tube and the vehicle, thereby to increase the cross-sectional area of tube or to decrease the cross-sectional area of the vehicle. This results in the increment of the construction cost of tube or decrement of the payload of the vehicle. The third is the suction of the flow in front of the vehicle by air compressor which transfers the high pressure air to the rear of the vehicle. However, when using a compressor, the structure of the vehicle becomes complicated and there is a drawback that the passenger's boarding space is reduced. Also, for the calculation, a complex flow simulation is required which considers the fluid suction by the compressor. Therefore, the successful development of transonic vehicle-evacuated tube system requires many researches concerning the relation between BR, $Mach_v$ of the vehicle, Kantrowitz limit and drag of the vehicle.

2.3 Construction of the axisymmetric grid and main parameters

The transonic vehicle was defined with reference to the specifications of the Hyperloop Alpha conceptual design [7] as Fig. 3; the reference area is about 1.4 m^2 and the total length of the vehicle is about 27 m. The distribution of the cross-sectional area was obtained from the longitudinal direction of the vehicle and then, axisymmetric radius of the vehicle was obtained as Fig. 4; the maximum radius of the vehicle is 0.67 m. Here, our concern is a parametric study of aerodynamic performance about a given vehicle shape inside the tube system; unlike the Hyperloop Alpha design, compressor was not considered during the axisymmetric computations for the computational efficiency. The radius of the tube was varied to meet the given BR between the vehicle and the tube and the length of the tube was set to be at least 10 times longer than the length of the vehicle. The final axisymmetric grid and the grid at the front and rear of

Fig. 3. Three dimensional geometry of the transonic vehicle

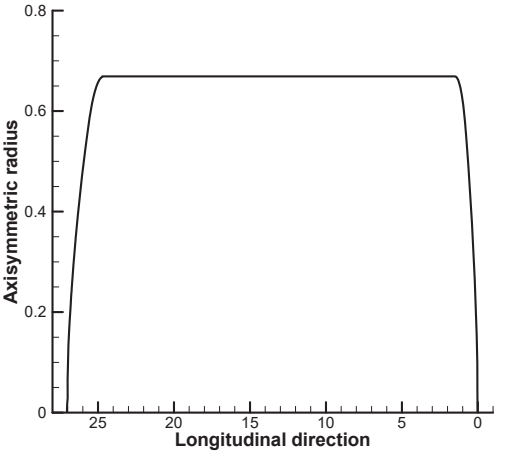

Fig. 4. Axisymmetric radius of the vehicle

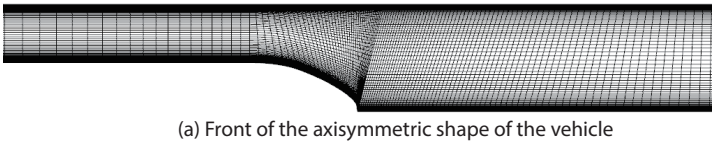

(a) Front of the axisymmetric shape of the vehicle

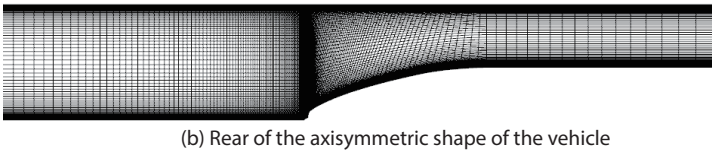

(b) Rear of the axisymmetric shape of the vehicle

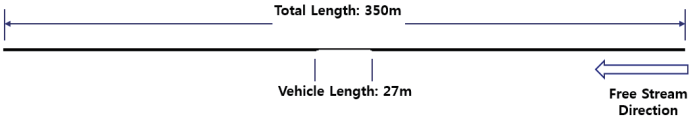

(c) Entire computational domain

Fig. 5. Axisymmetric grid

the vehicle are shown in Fig. 5.

In this study, Fluent, a commercial software, was used for steady-state flow analysis. Here, the speed of vehicle should be tested up to transonic speed, so density based solver which is suitable for high speed flow is used. For the boundary condition, the pressure-far-field condition in which no pressure reflection occurs at the boundary is used at the tube inlet and the pressure outlet condition is at the tube outlet [11]. For turbulence model, k-ω SST model, which is known for handling separated flows and adverse pressure gradients well, was used and the Y+ of the wall region was set as $O(1)$.

Concerning the main variables in this research were the BR, $Mach_v$ and Pre_t; first, BR was satisfied by fixing the cross-sectional area distribution of the vehicle and varying the radius of tube. The tube radius was set to 2.1 m, 1.5 m, and 1.1 m when BR was 0.1, 0.2, and 0.4, respectively. In the case of Pre_t, three cases were selected as 100 Pa, 1,000 Pa and 10,000 Pa, and $Mach_v$ was tested in eight conditions of Mach number 0.3 to 1; the total number of analysis cases was 72. Table 1 summarizes the main parameters and the testing conditions of each.

2.4 Results of axisymmetric simulations

Steady state flow analysis was carried out by varying the $Mach_v$, at given BR and Pre_t. Then, the pressure along the tube wall and C_d variation at BR = 0.2 and Pre_t=100 Pa was shown in Fig. 6-7 and C_d and Drag for each Mach number were summarized in Table 2. In Fig. 6, the vehicle was located between -27 and 0, and the direction of the vehicle was to the right. It can be seen that the pressure rise due to compression wave appears at the front of the vehicle and the pressure drop due to the flow expansion is well expressed at the rear part of the vehicle. Here, when BR = 0.2, the calculated Kantrowitz limit was Mach number of 0.675. In Fig. 7, it was shown that the $Mach_{local}$ increased while the flow passed by the vehicle and it exceeded 1 at rear of the vehicle at $Mach_v$=0.7, near the Kantrowitz limit. Thus in Fig. 8, the C_d is maximized at Mach number 0.7, which confirms that the Kantrowitz limit is satisfied well. However, when the Mach number is 0.7 or more, the C_d value tends to decrease continuously.

More specifically, as shown in Table 2, the coefficients of viscous drag (C_d, viscous) was continuously decreased with

Table 1. Main parameters and testing variables of each

Parameters	Testing conditions
BR	0.1, 0.2, 0.4
Pre_t (pa)	100, 1000, 10000
$Mach_v$	0.3 – 1.0

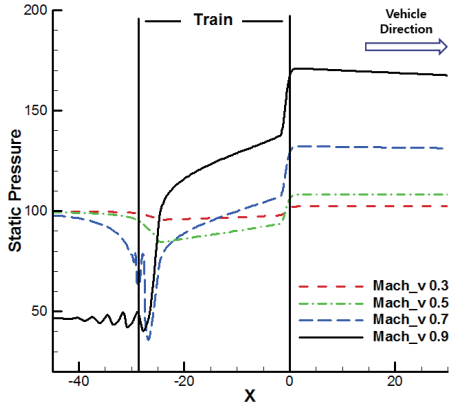

Fig. 6. Pressure distribution along tube wall at BR = 0.2, Pre_t = 100 Pa

Fig. 7. Comparison of Machlocal around the train

Table 2. C_d and Drag, BR = 0.2, evacuation pressure = 100 Pa

$Mach_v$	$C_{d,\ pressure}$	$C_{d,\ viscous}$	C_d	Drag (N)
0.3	0.5802	0.7303	1.3105	11.6
0.4	0.6326	0.6842	1.3167	20.8
0.5	0.7885	0.6548	1.4432	35.6
0.6	1.2527	0.6237	1.8764	66.6
0.7	2.0620	0.5529	2.6149	126.4
0.8	1.9389	0.4831	2.4219	152.9
0.9	1.7370	0.4418	2.1788	174.1
1.0	1.5958	0.4127	2.0085	198.1

respect to the increment of $Mach_v$ due to the increment of Re. Near the Kantrowitz limit, the pressure drag was maximized, and decreased over the Mach number of 0.7, then the total C_d value was decreased. If the $Mach_v$ is lower than the Kantrowitz limit, the $Mach_{local}$ around the vehicle does not exceed 1. However, if the $Mach_v$ is above the Kantrowitz limit, the $Mach_{local}$ around the vehicle becomes 1 or more and C_d decreased, which showed the typical transonic flow pattern around the Kantrowitz limit.

This tendency is the same at all BR and Pre_t as shown in Fig. 9. That is, when BR is 0.1, the Kantrowitz limit becomes 0.751, and the C_d continuously increases near this speed. In case of BR=0.4, the Kantrowitz limit is 0.583 and the overall C_d increases until $Mach_v$ became 0.7; the $Mach_v$ in which the C_D starts to decrease seems to be slightly delayed compared to the BR of 0.1 or 0.2. The cause of this phenomenon is due to the increase of BR and the generation of strong compression wave in front of the vehicle. In other words, when BR is large, the effective area for flow becomes narrowed and strong compression wave is generated in front of the vehicle in order to generate the inflow to move to the rear part of the vehicle inside of the tube as shown in Fig. 10; when the BR is 0.2, the pressure rise is 15.6 Pa, whereas when BR is 0.4, the pressure rise becomes 24.4 Pa. If a strong compression wave is formed at the front part of the vehicle, $Mach_{in}$ in front of the vehicle decreases to satisfy the energy conservation. Even if the $Mach_v$ exceeds the Kantrowitz limit, $Mach_{in}$ can be below the limit as shown in Fig. 11. Therefore, the C_d continuously increases until the $Mach_{in}$ exceeds the Kantrowitz limit.

Figure 12 summarize the results of pressure and viscous C_d at Pre_t=100 Pa in order to investigate the change in C_d with changes in BR. In Fig. 12, at the same $Mach_v$, it can be seen that the C_d values due to the viscous drag and the pressure drag decrease as BR decreases. Generally, the viscous drag of a vehicle is mainly generated in a long side of the vehicle, and the pressure drag is caused by the pressure difference between the front and rear of the vehicle. At this time, when the BR is reduced, the area through which the flow between the vehicle and the tube is passed increases and the flow acceleration around the vehicle decreases, which also reduces the magnitude of the coefficients of viscous drag. In addition, when the BR becomes smaller, the compressibility

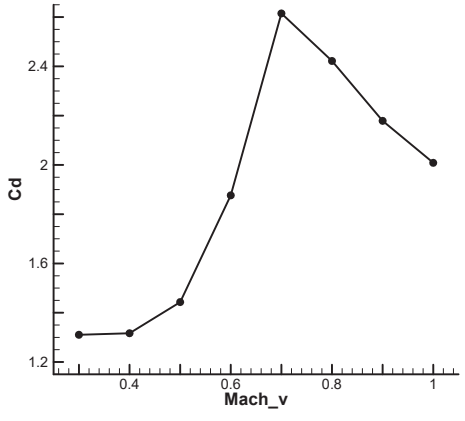

Fig. 8. C_d variation at BR = 0.2, Pre_t = 100 Pa

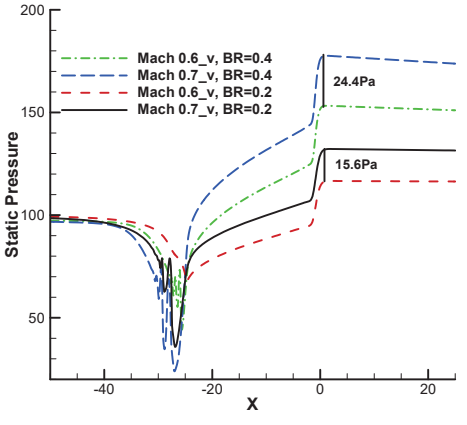

Fig. 10. Comparison of pressure difference according to BR, Pre_t = 100 Pa

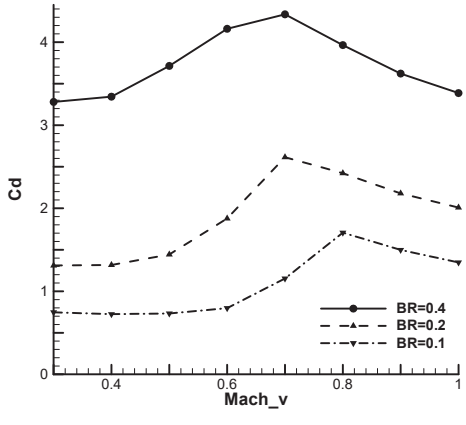

Fig. 9. Comparison of C_d variation according to BR, Pre_t = 100 Pa

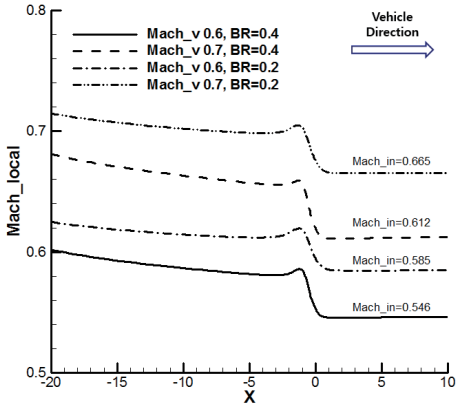

Fig. 11. Comparison of Mach number variation at tube wall, Pre_t = 100 Pa

effect of the air also becomes smaller and the pressure difference between the front and rear of the vehicle decreases as Fig. 10, which reduces the coefficient of the pressure drag. Therefore, the overall C_d is reduced when the BR decreases; at a transonic speed of about 0.7 to 0.9 and Pre_t=100 Pa, the C_d increased by about 30 - 40 % when the BR was doubled. It can be seen that this phenomenon is the same at different Pre_t conditions.

In case of same BR, the change in drag and C_d according to Pre_t in the tube is shown in Fig. 13. As the Pre_t became larger, the air density inside the tube linearly increased. However, the drag was not linearly increased according to the Pre_t; it increased by about 8 times when the Pre_t was 10 times at the $Mach_v$ of 0.7 to 0.9 and BR of 0.4 as shown in Fig. 13(a). It is because low Pre_t resulted in the decrease of Re and increase of C_d as Fig. 13(b). At $Mach_v$ about 0.7 to 0.9 and BR of 0.4, the C_d decreased asymptotically to the values of C_d at atmospheric pressure as the Pre_t increased. The decreasing rate of C_d was reduced as the Pre_t approached to the atmospheric pressure or BR decreased. Therefore, from the results of Pre_t and C_d, it is possible to estimate that drag increased as 8 – 8.5 times when the Pre_t increased 10 times with large BR and low Pre_t conditions.

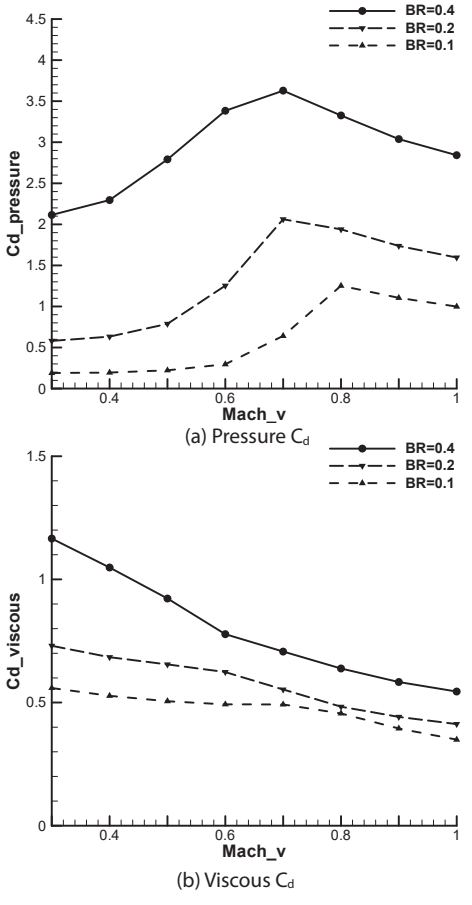

Fig. 12. Comparison of pressure and viscous C_d variation, Pre_t = 100 Pa

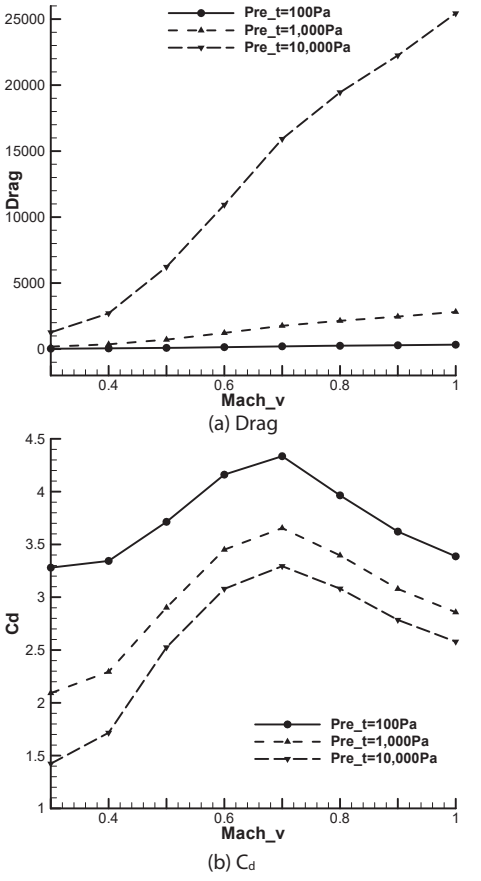

Fig. 13. Comparison of drag and C_d according to evacuation pressure, BR=0.4

3. Three dimensional flow simulations of transonic vehicle-evacuated tube system

In order to evaluate the actual C_D of the transonic vehicle, three dimensional flow field analysis was performed. At this time, the vehicle shape for the calculation of the three dimensional flow field was shown in Fig. 3; the reference area is the same as the axisymmetric cases about 1.4 m^2 and the total length of the vehicle is about 27 m. Here, the grid should be densely distributed around the vehicle, and the shape of the aligned grid is advantageous in the far region from the vehicle in order to maintain the flow information without dissipation. Therefore, the entire computational domain is divided into the internal region near vehicle and outer tube region as Fig. 14. At the boundary of inner and outer region, the interface boundary conditions were used which use non-conformal grid and allow the exchange of flow information. On the surface of the vehicle, triangular and square lattices were mixed as Fig. 15. In the case of the boundary layer, the distance from the vehicle surface to the first layer was 0.5

mm, and 20 layers constituted the boundary layer. After that, the tetrahedral grid was used to densely distribute the lattice around the inner vehicle. The outer region was created by extruding the lattice of the interface in the longitudinal direction of the vehicle. As a result, the total number of grids was composed of approximately 3,920,000 unstructured grids and the Y + value on the vehicle surface was set about $O(1)$.

The BR and Pre_t were determined as the specifications of the Hyperloop Alpha document; the BR was 0.36 with the Kantrowitz limit of 0.596 and the Pre_t was 100 Pa. Steady state flow analysis was performed using a density based solver by adjusting the $Mach_v$ varied from 0.3 to 1.0. Similar to the boundary conditions used in axisymmetric analyses, the pressure-far-field condition is used at the tube inlet and the pressure outlet condition is at the tube outlet. And k-ω SST model was used for the calculation of turbulence. After the three dimensional flow calculations, the results were compared with those of axisymmetric ones.

The C_D and drag obtained from the analysis are shown in Table 3 and Fig. 16, respectively. The overall tendency between the results of axisymmetric and three dimensional

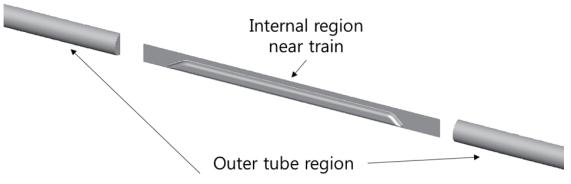

Fig. 14. Construction of entire computational domain

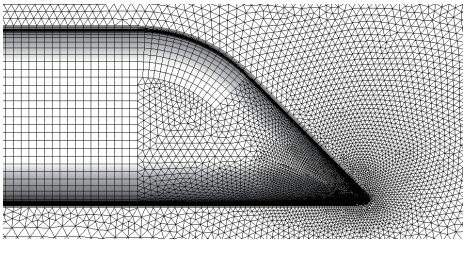

Fig. 15. Surface grid of the vehicle

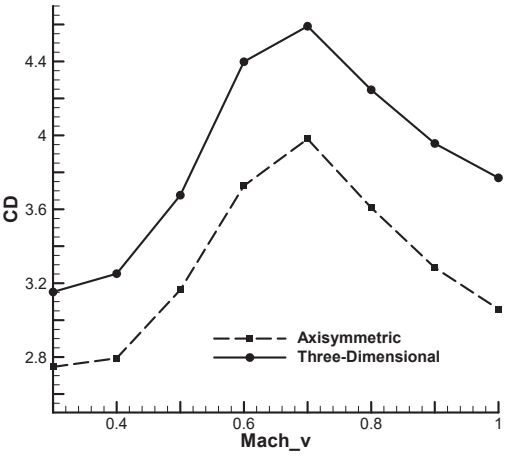

Fig. 16. Comparison of CD between axisymmetric and 3D results

flow simulations are very similar. Similar to the axisymmetric cases of BR 0.4, a strong compression wave in front of the vehicle results in the decrease of $Mach_{in}$ in front of the vehicle below the Kantrowitz limit and the $Mach_v$ which Cd values started to decrease increased over the Kantrowitz limit. The quantitative difference of C_D value can be recognized between the axisymmetric and the three dimensional flow simulations. It is because the real vehicle is located eccentrically in the tube; the effective area of the flow at the bottom of the vehicle is reduced and stronger compression wave is formed in front of the vehicle than that of axisymmetric cases. However, since the tendency of the CD variation is similar to the axisymmetric one, it is possible to utilize the axisymmetric calculations with changing the main parameters in the initial design stage, and to calibrate the results by the three dimensional simulations.

4. Conclusion

In this study, the aerodynamic C_d and drag variation

Table 3. Results of axisymmetric and 3D, BR = 0.34, evacuation pressure = 100 Pa

$Mach_v$	Axisymmetric		3D	
	C_d	Drag (N)	C_D	Drag (N)
0.3	2.7468	24.4	3.1526	14.19
0.4	2.7939	44.1	3.2515	26.02
0.5	3.1638	78.0	3.6762	45.97
0.6	3.7272	132.3	4.3985	79.20
0.7	3.9806	192.4	4.5389	95.91
0.8	3.6085	227.8	4.5905	112.50
0.9	3.2841	262.4	4.2464	135.92
1.0	3.0596	301.8	3.9562	160.27

according to the main design parameters of the transonic vehicle-evacuated tube system such as $Mach_v$, BR and Pre_t were examined through steady state axisymmetric calculations.

First, as $Mach_v$ increased, C_d was maximized near Kantrowitz limit and decreased beyond Kantrowitz limit, which showed the typical transonic flow pattern. However, in case of large BR, the $Mach_v$ at which C_d became maximum exceeded beyond the Kantrowitz limit. It was because large BR caused the strong compression wave in front of the vehicle and the wave made $Mach_{in}$ below the Kantrowitz limit though $Mach_v$ exceeded the limit.

Second, as the BR decreased, the aerodynamic drag of the vehicle was reduced. This was because when the BR was small, the area between the vehicle and the tube was widened, the flow acceleration around the vehicle decreased and the coefficients of viscous drag also diminished. In addition, compression wave in front of the vehicle were weakened and the coefficients of pressure drag were reduced; at $Mach_v$ of 0.7 to 0.9 and Pre_t of 100 Pa, the C_d increased by about 30 - 40 % when the BR was doubled.

Third, as the Pre_t increased, the overall aerodynamic drag of the vehicle increased because of the increment of air density. However, the C_d decreased as Pre_t increased; the drag increased as 8 – 8.5 times when the Pre_t increased 10 times with large BR and low Pre_t conditions. Based on these results, three dimensional flow simulations were performed with vehicle under the conditions of BR of 0.36 and Pre_t of 100 Pa. It was confirmed that the overall tendency of the C_D variation was the same between axisymmetric and three dimensional results except the quantitative values of C_D. These results can be used as basic data for future development of transonic vehicle – evacuated tube system.

Acknowledgement

The research was supported by a grant from the Academic Research Program of Korea National University of Transportation in 2014.

References

[1] Goddard, R. H., "The Limit of Rapid Transit", *Scientific American*, Vol. 101, No. 21, 1909, pp. 366. DOI: 10.1038/scientificamerican11201909-366d

[2] Trzaskoma, W. P., Tube Vehicle System (TVS) Technology Review, 1970, No. M70-4 Intrm Rpt.

[3] Bierlaire, M., Axhausen, K. and Abay, G., "The Acceptance of Modal Innovation: The Case of Swissmetro", *In Proceedings of the 1st Swiss Transportation Research Conference*, 2001.

[4] Shen, Z. Y., "On Developing High-Speed Evacuated Tube Transportation in China", *Journal of Southwest Jiaotong University*, Vol. 40, No. 2, 2005, pp. 133-137.

[5] Sato, Y., Konagai, K., Maeda, T., Saito, S., Satoh, T. and Ishida, M., "SUPERMETRO-Super-High-Speed-Train in Low Pressure Tunnel", *World Congress on Railway and Research*, 2006.

[6] Lee, H. W., Cho, S. Y., Cho, W. Y., Lee, J. and Kwon, H. B., "Analysis of the Magnetic Effect on the Tube Infrastructure for a Super Speed Tube Train", *International Journal of Railway*, Vol. 2 No. 4, 2009, pp.170-174.

[7] Musk, E., "Hyperloop Alpha", SpaceX. Retrieved August 13 2013.

[8] Kantrowitz, A. and Donaldson, C. D., "Preliminary Investigation of Supersonic Diffusers", *National Advisory Committee on Aeronautics, Langley Memorial Aeronautical Laboratory, Langley Field, Virgini*a, 1945.

[9] Opgenoord, M. J. and Caplan, P. C., "On the Aerodynamic Design of the Hyperloop Concept", *In Proceedings of the 35th AIAA Applied Aerodynamic Conference*, 2017.

[10] Van Wie, D. M., Kwok, F. T. and Walsh, R. F., "Starting Characteristics of Supersonic Inlets", AIAA paper 96-2914, 1996.

[11] ANSYS FLUENT 12.0 Theory Guide.